Chinese Chemical Letters 34 (2023) 107574

Contents lists available at ScienceDirect

Chinese Chemical Letters

journal homepage: www.elsevier.com/locate/cclet

Redox-responsive phenyl-functionalized polylactide micelles for enhancing Ru complexes delivery and phototherapy

Maomao He[a], Zongwei Zhang[a], Ziyue Jiao[a], Meiyu Yan[a], Pengcheng Miao[a], Zhiyong Wei[a], Xuefei Leng[a], Yang Li[a,*], Jiangli Fan[a,b], Wen Sun[a,b,*], Xiaojun Peng[a]

[a] State Key Laboratory of Fine Chemicals, Liaoning Key Laboratory of Polymer Science and Engineering, Dalian University of Technology, Dalian 116024, China
[b] Ningbo Institute of Dalian University of Technology, Ningbo 315016, China

ARTICLE INFO

Article history:
Received 2 April 2022
Revised 27 May 2022
Accepted 31 May 2022
Available online 3 June 2022

Keywords:
PEG-PLA micelles
Phenyl functionalization
Redox-responsive
Ru complexes
Delivery

ABSTRACT

Poly(ethylene glycol)-poly(lactic acid) block copolymer (PEG-PLA) is one of the most widely used biomedical polymers in clinical drug delivery owing to its biocompatibility and biodegradability. However, endowing PEG-PLA micelles with high drug loading, self-assembly stability and fast intracellular drug release is still challenging. Redox-responsive diblock copolymers (MPEG-SS-PMLA) of poly(ethylene glycol) and phenyl-functionalized poly(lactic acid) with disulfide bond as the linker are synthesized to prepare PLA-based micelles that demonstrate excellent colloidal stability and high Ru loading. Notably, MPEG-SS-PMLA achieved a remarkably high Ru loading efficiency of 84.3% due to the existence of strong π-π stacking between phenyl and Ru complex. MPEG-SS-PMLA exhibited good colloidal stability in physiological condition but quickly destabilized by reductive tumor microenvironment. Interestingly, about 74% of Ru complex was released under 10 mmol/L GSH concentration. Ru-loaded MEPG-SS-PMLA showed efficient delivery and release of Ru complex into MCF-7 cancer cells, achieving enhanced *in vitro* and *in vivo* antitumor activity of photodynamic therapy. This feasible functionalization method of MPEG-PLA has appeared to be a clinically viable platform for controlled delivery therapeutic agents and enhanced phototherapy.

Photodynamic therapy (PDT) is a promising noninvasive approach for cancer therapy by combining photosensitizer (PS), oxygen (O_2) and light to generate reactive oxygen species (ROS), which cause cellular death [1–4]. Transition metal complexes and in particular Ru(II) polypyridyl complexes were found to be extremely promising on account of their long-lasting triplet excited states available to generate ROS, with one example starting phase II clinical trials for the treatment of bladder cancer [5–7]. However, the most critical limitation to the application of Ru(II) polypyridyl complexes in PDT is their limited ability to cross the cell membrane due to their high hydrophilicity and positive charge [8]. Meanwhile, the Ru(II) polypyridyl complexes accumulate also in healthy tissue and it is practically impossible to expose only the tumor to the light source. Therefore, healthy tissues are also damaged during PDT. To overcome this drawback, a variety of Ru(II) polypyridyl complexes delivery systems have been reported, including polymeric nanoparticles, mesoporous silica nanoparticles, carbon nanotubes, metal-organic frameworks, and so on [9]. Ideally, a viable Ru(II) polypyridyl complexes delivery system should be able to prevent aggregation and improve water solubility; enhance site-selectivity to the tumor; and maintain chemical stability. Within this context, attention has been focused on the application of polymeric nanoparticles due to their biocompatibility, low cost of production/isolation, and versatility [10–16]. Recent studies have demonstrated that the polymeric nanoparticles containing Ru(II) polypyridyl complexes are able to selectively accumulate at tumor sites through the enhanced permeability and retention (EPR) effect, therefore enhancing PDT treatment specificity and reducing undesired side effects [8,17–20].

Among a wide range of polymers, biodegradable aliphatic polyesters and especially polylactide (PLA) are the most commonly used for sustained and targeted delivery of different therapeutic agents due to their biocompatibility and biodegradability [21,22]. A typical example of PLA copolymers is a clinically approved poly(ethylene glycol)-polylactide (PEG-PLA) copolymer micelles loaded with anticancer drug (Genexol PM) for the treatment of various malignant tumors [23]. Despite the great potential of

* Corresponding author at: State Key Laboratory of Fine Chemicals, Liaoning Key Laboratory of Polymer Science and Engineering, Dalian University of Technology, Dalian 116024, China.
E-mail addresses: liyang@dlut.edu.cn (Y. Li), sunwen@dlut.edu.cn (W. Sun).

https://doi.org/10.1016/j.cclet.2022.05.088
1001-8417/

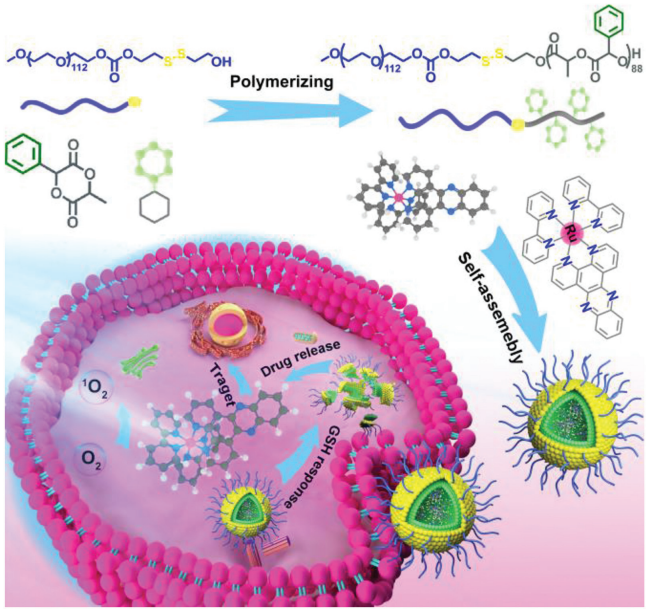

Fig. 1. Schematic illustration of biodegradable Ru-containing polylactide MPEG-SS-PMLA@Ru micelles for enhanced Ru(II) polypyridyl complexes delivery and cancer phototherapy.

PEG-PLA, there are several challenges that remain to be overcome for their clinical applications. First, the majority of PLA-based micelles have low drug loading efficiency [24,25]. This would increase the time of intravenous injection required to achieve the same effect. Second, polymeric micelles tend to disintegrate or aggregate in the blood stream due to insufficient stability [26]. Third, the therapeutic agents can hardly be released in the tumor microenvironment, which usually attenuates treatment effect [27–29]. All these problems hinder the clinical performance of PEG-PLA.

Increasing the interactions between the cores of polymeric micelles and therapeutic agents can enhance the thermodynamic driving force for drug loading and the micellar stability among the different major driving forces in the supramolecular self-assembly procedures [30–37]. Introducing aromatic groups onto the side chain of aliphatic polyesters is a common approach to induce the π-π stacking interaction between polymeric micelles and anticancer drugs. Herein, we explored a novel phenyl-functionalized poly(ethylene glycol)-polylactide block copolymers (MPEG-SS-PMLA) and their self-assembled micelles for ultra-high loading and rapidly reduction-responsive release of Ru(II) polypyridyl complexes, $[Ru(bpy)_2dppz][PF_6]_2$ (bpy = 2,2-bipyridine; dppz = dipyridophenazine), as a PDT photosensitizer (Fig. 1). The polymer consists of hydrophilic PEG block and phenyl-modified PLA hydrophobic block linked through a reduction-sensitive disulfide bond, which is easily degraded by high concentrations of glutathione (GSH) in the cytoplasm of the tumor cells. Importantly, PMLA blocks are composed of lactic acid and natural mandelic acid possess pendant groups on side chains alternately connected by ester bonds, which would largely improve drug loading and micellar stability *via* π-π stacking. MPEG-SS-PMLA could self-assemble into supramolecular micelles with high stability in physiological conditions and were effectively internalized into tumor cells. Subsequently, cytoplasmic reductant induced the cleavage of the disulfide bond, resulting in disintegration of the micelles, with a rapid release of Ru complexes. The release of the anticancer drug-Ru complex conjugates was accompanied by the generation of singlet oxygen ($^1O_2$) under light, resulting in enhanced phototherapy effects.

The synthetic procedure of MPEG-disulfide-OH initiator (MPEG-SS-OH) and redox-responsive MPEG-SS-PMLA block copolymer is shown in Scheme 1a. At first, the terminal hydroxyl of methoxy poly(ethylene glycol) was capped with 1,1′-carbonyldiimidazole (CDI) to obtain CDI-functionalized MPEG-CDI. In the ^{1}H NMR spectrum, the newly emerged characteristic signals at ~7.08, 7.45 and 8.15 ppm are attributed to the proton signals of the imidazole group. MPEG-CDI was further reacted with 2-hydroxyethyl disulfide to produce the disulfide-containing MPEG-SS-OH. The proton signals of the hydroxyethyl disulfide groups appeared at 2.94 and 4.35 ppm, which were accompanied by the disappearance of the proton signals of the imidazole group, indicating the successful synthesis of the MPEG-SS-OH (Fig. 2a). Meanwhile, the phenyl-functionalized lactide monomer (MLA) was synthesized *via* a two-step route. First, natural and commercially available mandelic acids

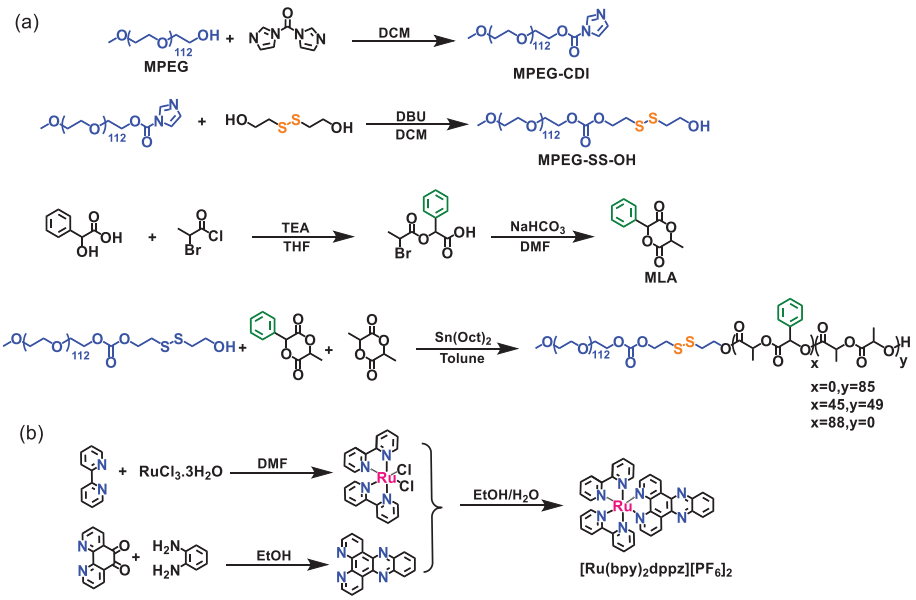

Scheme 1. The synthetic process of (a) the amphiphilic methoxy poly(ethylene glycol)-SS-poly(mandelic-*co*-lactic acid) block copolymer (MPEG-SS-PMLA) and (b) the hydrophobic ruthenium(II) polyridyl complexes, $[Ru(bpy)_2dppz][PF_6]_2$.

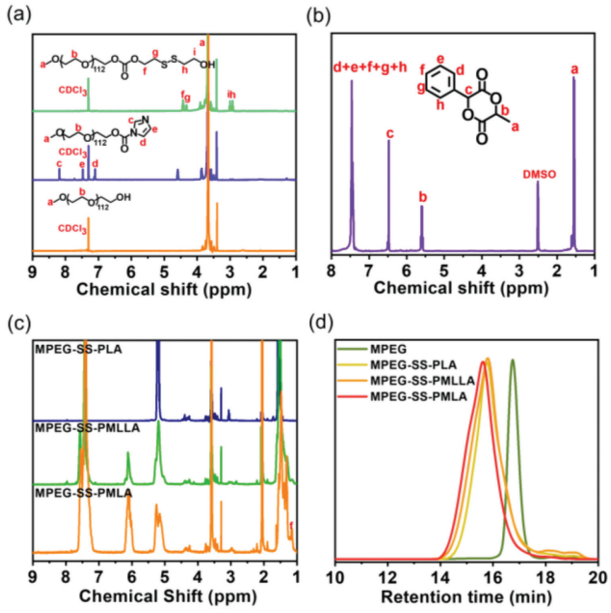

Fig. 2. Characterization of the poly(ethylene glycol)-functionalized polylactide block copolymers MPEG-SS-PMLA. (a) ^{1}H NMR spectra recorded in $CDCl_3$ for the MPEG, MPEG-CDI and MPEG-SS-OH polymers. (b) ^{1}H NMR spectrum recorded in $CDCl_3$ for the phenyl-functionalized monomer. (c) GPC spectra recorded in DMF for the MPEG-SS-OH, MPEG-SS-PLA, MPEG-SS-PMLLA and MPEG-SS-PMLA copolymers. (d) ^{1}H NMR spectra recorded in $CDCl_3$ for the MPEG-SS-PLA, MPEG-SS-PMLLA and MPEG-SS-PMLA copolymer.

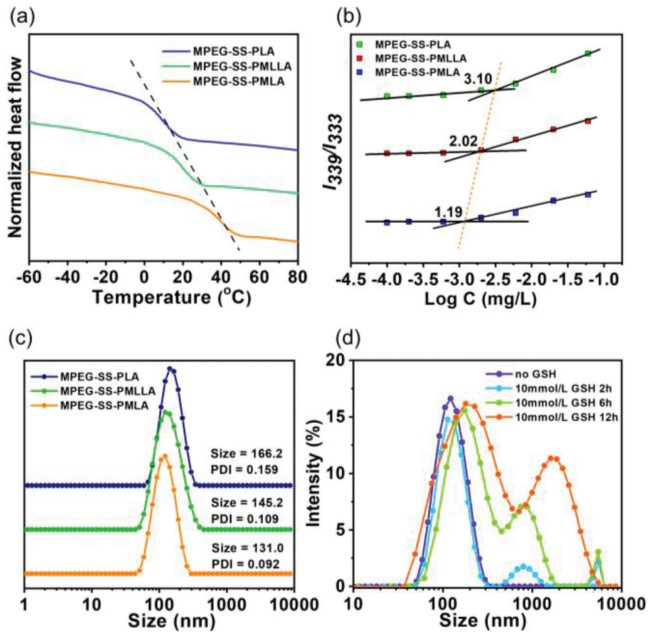

Fig. 3. Characterization of the MPEG-SS-PMLA micelles. (a) DSC spectra of for the MPEG-SS-PLA, MPEG-SS-PMLLA and MPEG-SS-PMLA copolymers. (b) CMC determination plot of the intensity ratio of I_{339}/I_{333} from pyrene excitation spectra versus the logarithm of MPEG-SS-PLA, MPEG-SS-PMLLA and MPEG-SS-PMLA copolymers concentration. (c) The diameter of MPEG-SS-PLA, MPEG-SS-PMLLA and MPEG-SS-PMLA copolymer micelles determined by dynamic light scattering (DLS). (d) Size changes of the MPEG-SS-PMLA copolymer micelles at different GSH concentrations.

reacted with 2-bromopropionyl chloride to form a halogenated carboxylic acid intermediate. Subsequently, the intermediate underwent intramolecular cyclization in the presence of $NaHCO_3$ to obtain the final monomer MLA (Fig. 2b and Fig. S1 in Supporting information). Then, the ring opening polymerization (ROP) of MLA initiated with MPEG-SS-OH at 120 °C in toluene yielding the final copolymer MPEG-SS-PLA, MPEG-SS-PMLLA, and MPEG-SS-PMLA. The preparation process for $[Ru(bpy)_2dppz][PF_6]_2$ is illustrated in Scheme 1b. Briefly, dppz and *cis*-$[Ru(bpy)_2Cl_2]$ were synthesized as previously reported. These two compounds were then mixed together and reflexed to form $[Ru(bpy)_2dppz][PF_6]_2$. Results from ^{1}H NMR, ^{13}C NMR spectra, and electrospray ionization mass spectrometry (ESI-MS) revealed that the synthesis was successful (Figs. S2–S5 in Supporting information).

The peaks in ^{1}H NMR spectra of MPEG-SS-PLA, MPEG-SS-PMLLA, and MPEG-SS-PMLA are well assigned to the corresponding proton signals (Fig. 2c and Figs. S6-S8 in Supporting information). Moreover, the area ratios integrated from the proton peaks are remarkably consistent with the theoretical calculating values according to different monomer feedings, which also illustrates the good controllability of the anionic ring-opening polymerization. The molecular weights ($M_{n,NMR}$) of the amphiphilic block copolymers were calculated from the integrated areas of methylene hydrogens of the ethylene oxide (3.59 ppm, of MPEG blocks), and two methine hydrogen of the lactic acid and mandelic acid units (5.19 and 6.10 ppm, of PLA blocks). As shown in Table S1 (Supporting information), the three copolymers MPEG-SS-PLA, MPEG-SS-PMLLA, and MPEG-SS-PMLA demonstrated the $M_{n,NMR}$ values of 17.4, 21.5, and 23.3 kg/mol. Additionally, the theoretical proportion of MLA and LA in MPEG-SS-PMLLA are 50/50, respectively, which are roughly consistent with the values of 49/45 measured by ^{1}H NMR spectra.

The molecular weights of these block copolymers were further evaluated by gel permeation chromatography (GPC) analyzes (Fig. 2d). The GPC curves of MPEG-SS-PLA, MPEG-SS-PMLLA, and MPEG-SS-PMLA strictly monomodal and symmetric, demonstrating uniform composition. Relative to MPEG, the curves of MPEG-SS-PLA, MPEG-SS-PMLLA, and MPEG-SS-PMLA apparently shift toward left, suggesting the increase of molecular weights. The ranking sequences of Mn, GPCs for MPEG-SS-PLA, MPEG-SS-PMLLA, and MPEG-SS-PMLA agree well with those of $M_{n,NMR}$, whereas the value of $M_{n,GPC}$ for each sample is slightly larger than that of $M_{n,NMR}$ due to the molecular weights from GPC are relative values using the linear polystyrene as a standard. This ingenious synthesis method provides enormous controllability to design and synthesize PLA materials with well-defined structures and functions for biomedical applications.

The differential scanning calorimetry (DSC) was used to investigate the effect of π-conjugated phenyl moieties on the mobility of MPEG-PLA diblock copolymer chains (Fig. 3a). In the DSC spectra, the glass transition temperature (T_g) of the three diblock copolymers were tested, the T_g increased with the sequence of MPEG-SS-PLA, MPEG-SS-PMLLA, and MPEG-SS-PMLA. The π-conjugated phenyl moieties enhanced the intermolecular forces between polymeric chains, limiting the movement of the polymer chains. The addition of π-conjugated phenyl moieties also improved the thermal stability of the polymers, since higher temperatures were required for their thermal decomposition (Fig. S9 in Supporting information). The results revealed that the π-conjugated phenyl moieties could increase the interaction between polymeric chains, which would be beneficial for the improvement of drug loading and stability of polymeric micelles.

The three block copolymers were amphiphiles, which could self-assemble into micelles in aqueous solution. The quantitative micellization of polymers was determined by critical micelle concentration (CMC), which indicated the stability of polymeric micelles. The CMCs of MPEG-SS-PLA, MPEG-SS-PMLLA and MPEG-SS-PMLA micelles were 3.10, 2.02 and 1.19 mg/L (Fig. 3b), respectively. The CMC of polymeric micelles gradually decreases with the increasing number of phenyl moieties on the PLA side chains. The π-conjugated phenyl moieties in MPEG-PLA block copolymers de-

creased the CMC could be perhaps explained by more conjugated hydrophobic architectures. The mean hydrodynamic diameters of the three blank polymeric micelles were measured by dynamic light scattering (DLS) spectrometer (Fig. 3c). The three micelles were monodispersed with the mean diameters of 166.2, 145.2 and 131.0 nm. The polydispersity indexes for blank MPEG-SS-PLA, MPEG-SS-PMLLA and MPEG-SS-PMLA micelles were 0.159, 0.109 and 0.092. All the mean hydrodynamic diameters of blank micelles were reduced with the increasing the number of phenyl moieties on the PLA side chains. The reduction sequences were MPEG-SS-PLA, MPEG-SS-PMLLA and MPEG-SS-PMLA. MPEG-SS-PMLA exhibited the smallest diameter in blank micelles, suggesting a strongest hydrophobic intermolecular interaction.

Next, the redox-response of the MPEG-SS-PMLA polymeric micelles was investigated by DLS and TEM tests. The polymeric micelle sizes were almost unchanged in the presence of 10 μmol/L GSH (the GSH level in the normal tissues), indicating that the core-shell structure was stable under normal physiological conditions (Figs. S10 and S11 in Supporting information). However, when the GSH concentration of micelle solution increases to 10 mmol/L (tumor microenvironment) for 2 h, the unimodal DLS curve began to form a bimodal distribution, and the phenomenon became even more obvious after 6 h. With the incubation time further prolonging to 12 h, the DLS curve demonstrated a significant unimodal distribution, and the size of the particles increased from the original 131.0 nm to 474.0 nm (Fig. 3d). These results indicated that the block copolymer chains gradually dissociated due to the cleavage of the disulfide linker by reduced GSH as the reaction time prolonged, and thus leading to the agglomeration of the hydrophobic PMLA segments and hydrodynamic diameter increase.

The Ru-loaded polymeric micelles (MPEG-SS-PMLA@Ru) were prepared by adding water to an acetonitrile (ACN) solution of MPEG-SS-PMLA and $[Ru(bpy)_2dppz][PF_6]_2$. Then, the organic solvent was removed *via* dialysis against water. When the feeding ratio of polymer to Ru was 5:1, the Ru loading content and encapsulation efficiency of unimolecular micelles were determined to be 14.4% and 84.3% for Ru complex, suggesting a high loading capacity of MPEG-SS-PMLA, which were better compared to the other copolymers and suitable for the delivery of Ru complex (Table S2 in Supporting information). The side chain modification of π-conjugated phenyl moieties could significantly improve the Ru loading (Fig. S12 in Supporting information). The MPEG-SS-PMLA@Ru micelles exhibited a monodisperse spherical morphology with a hydrodynamic diameter of 164.2 nm determined *via* DLS (Fig. 4a). TEM showed that the diameters of MPEG-SS-PMLA@Ru micelles were mainly distributed around 100 nm, which was comparable to the DLS result (Fig. 4b). Additionally, the metal-to-ligand charge transfer (MLCT) peak of the MPEG-SS-PMLA@Ru micelles was almost the same to that of the Ru complex, indicating that polymer encapsulation did not affect their optical properties (Fig. 4c).

In vitro releases of the MPEG-SS-PMLA@Ru micelles were studied under both simulated normal physiological and tumor microenvironment conditions by using a dialysis method (Fig. 4d). The micelle solution showed 44% release in 24 h, whereas MPEG-SS-PMLA@Ru exhibited relatively less Ru complex release at pH 7.4. However, in response to 10 mmol/L GSH, the Ru complex release rate at 24 h increased from 44% to 74%. Moreover, under the condition of 10 mmol/L GSH + pH 5.5, the redox and acid dual-response led to the cumulative release rate of Ru complex further increased to 81%. With the time prolonging to 48 h, the Ru complex release rate was over 92%. Additionally, after being treated in GSH-rich environments, the TEM image of MPEG-SS-PMLA@Ru showed that both the Ru-loaded micelles completely collapsed, which demonstrated that the Ru-loaded copolymer micelles are stable under normal physiological conditions, but experienced redox-triggered

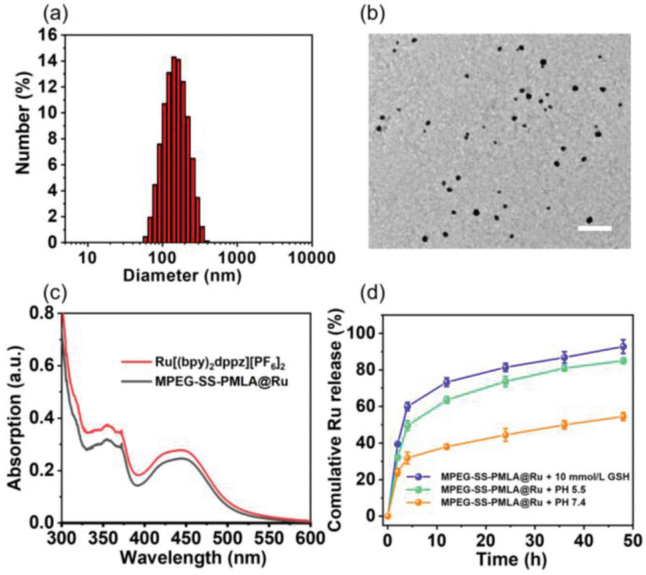

Fig. 4. Characterization of the MPEG-SS-PMLA@Ru micelles. (a) The diameter of MPEG-SS-PMLA@Ru polymeric micelles determined by DLS. (b) Transmission electron microscope (TEM) image of MPEG-SS-PMLA@Ru micelles (Scale bar = 500 nm). (c) Absorption spectral of $[Ru(bpy)_2dppz][PF_6]_2$ and MPEG-SS-PMLA@Ru micelles. (d) *In vitro* drug release of MPEG-SS-PMLA@Ru micelles in PBS with different treatment.

Ru complex release in the tumor microenvironment (Figs. S13 and S14 in Supporting information). These results demonstrated the redox responsiveness of the MPEG-SS-PMLA@Ru micelles for the release of the anticancer Ru complex. Meanwhile, the precise redox-triggered photosensitizer delivery would guarantee the improved therapeutic effect [38,39].

In cancer treatment, the cellular uptake efficiency of therapeutic agents is one of the key factors, determining the result of cancer treatment [12,40,41]. In the previous studies, low levels of Ru complexes internalization in cancer cells have been reported. Here, the cellular uptake of the Ru complex in MCF-7 cells was evaluated using confocal microscopy (Fig. 5a). Brighter red fluorescence was observed in the cells treated with MPEG-SS-PMLA@Ru micelles at the 12 h time point than free Ru complex, suggesting effective cellular uptake of the Ru-containing polymeric micelles. Since $^1O_2$ was required for PDT to kill cancer cells, intracellular $^1O_2$ generation was imaged by a cell-permeable green fluorescent probe (DCFH-DA). Negligible fluorescence was observed in the absence of sole MPEG-SS-PMLA@Ru micelles or light irradiation. Conversely, obvious green fluorescence signals were observed in MPEG-SS-PMLA@Ru micelles after light irradiation (Fig. 5b). These results clearly show that the light irradiation of polymeric micelles results in the intracellular generation of $^1O_2$.

Inspired by the above results, the cell viability of MPEG-SS-PMLA@Ru was evaluated using the 3-(4,5-dimethylthiazol-2-yl)-2,5-diphenyltetrazolium bromide (MTT) assay. MPEG-SS-PMLA micelles did not cause appreciable cytotoxicity to cell lines including 4T1 and MCF-7 cancer cells, indicating that the polymer micelles were reliable nanocarriers with high biosafety (Fig. 5c). However, cell viability was rapidly reduced in a concentration-dependent fashion for the cells treated with MPEG-SS-PMLA@Ru micelles upon light irradiation, with an IC_{50} of 8.4 μg/mL to MCF-7 cells (Fig. 5d and Fig. S15 in Supporting information). The frequency of cell apoptosis and death pathways induced by MPEG-SS-PMLA@Ru micelles were further examined (Fig. 5e). The survival rates of the control and light groups were above 94.0% and 93.7%, respectively, and few apoptosis signals were detected. When

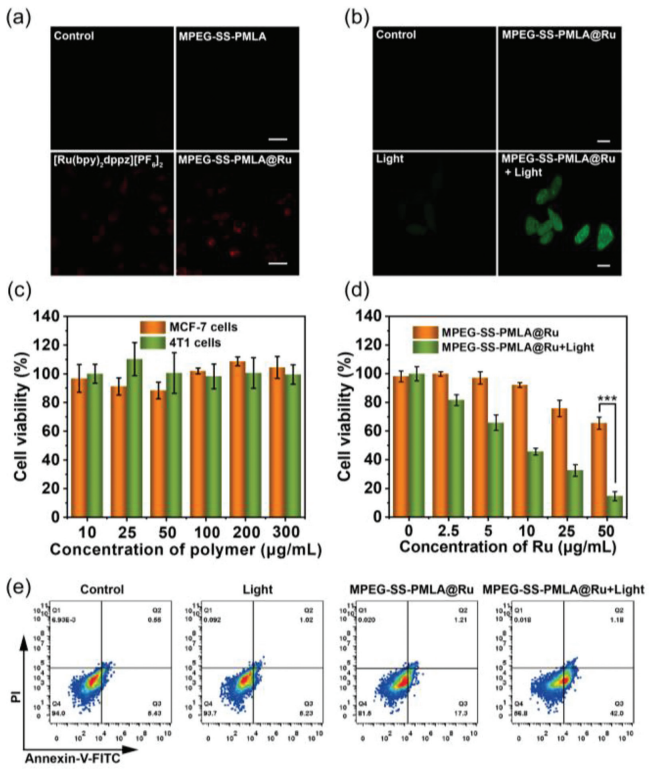

Fig. 5. Cellular internalization and *in vitro* antitumor activity of MPEG-SS-PMLA@Ru micelles in MCF-7 cancer cells. (a) Confocal fluorescence images of MCF-7 cells treated with MPEG-SS-PMLA@Ru micelles for 12 h (Scale bar = 50 μm). (b) Confocal fluorescence images of MCF-7 cells after incubation with for 12 h and staining with DCFH-DA, followed by light irradiation (Scale bar = 20 μm). (c) Cell viability of MCF-7 and 4T1 cells incubated with MPEG-SS-PMLA micelles at various concentrations for 24 h. (d) Cell viability of MCF-7 cells incubated with MPEG-SS-PMLA@Ru micelles at various concentrations under dark conditions and light irradiation (450 nm, 30 mW/cm^2) for 20 min. (e) Cell apoptosis of MCF-7 cancer cells determined by flow cytometry with different treatments.

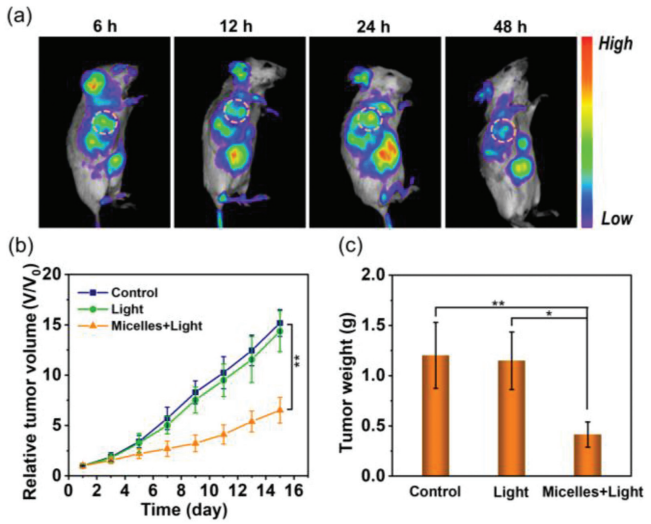

Fig. 6. *In vivo* antitumor efficacy in 4T1 tumor-bearing mice. (a) Fluorescence images of 4T1 tumor-bearing mice after intravenous injection of dye-loaded MPEG-SS-PMLA@Ru micelles. (b) The relative tumor volume changes with different treatments. (c) Average weights of tumors at two weeks after treatment.

treated with MPEG-SS-PMLA@Ru micelles, the higher proportions of cells were in the apoptosis stage (18.5%) compared to that of the control and light group. The apoptotic ratios significantly increased in the groups treated with light irradiation (450 nm, 30 mW/cm^2, 20 min), indicating that light significantly enhanced the antitumoral effects of the micelles. As expected, the cancer cells treated with MPEG-SS-PMLA@Ru micelles under light irradiation demonstrated the highest apoptosis rate (43.1%). These findings were consistent with the *in vitro* phototoxicity results, suggesting that the redox-triggered release of Ru complex and light-triggered production of $^1O_2$ led to enhanced cells death.

To examine the optimal time for accurate phototherapy, we investigated the accumulation of the polymeric micelles in the mouse breast cancer subcutaneous tumor model by *in vivo* fluorescence imaging at different time points (Fig. 6a). All animal experiments were performed in accordance with guidelines approved by the Ethics Committee of Dalian University of Technology (DUT20210902). After injecting dye-loaded MPEG-SS-PMLA@Ru micelles into the tail vein of mice, clear fluorescence signals can be observed in the tumor site at 6 h post-injection time. The fluorescence intensity at the tumor site gradually increased, reaching the maximum at 24 h, which was the best time point for light irradiation. Although the fluorescence intensity gradually decreased after 24 h due to the metabolic physiology of mice, fluorescence could be still observed at the tumor site even after 48 h.

Next, the *in vivo* antitumor activity was further examined by intravenously injecting MPEG-SS-PMLA@Ru micelles into 4T1 tumor-bearing mice, followed by local activation with 450 nm light (30 mW/cm^2, 60 min) after injection micelles for 24 h. Short-wavelength (blue or green) photosensitizer-loaded polymer micelles, although traditionally considered to be academic curiosities due to the low tissue penetration of visible light, are regaining interest for certain cancers such as skin and cervical cancer, because the thickness of these tumors matches the penetration depth of blue and green light [42]. The tumor volume of the control and light-only treatment groups showed rapid growth within 14 days. As expected, mice treated with MPEG-SS-PMLA@Ru micelles and light irradiation drastically slowed the tumor growth (Fig. 6b). After two weeks, the tumors were collected, weighed, and photographed (Fig. 6c and Fig. S16 in Supporting information). Similarly, MPEG-SS-PMLA@Ru micelles with light irradiation demonstrated the efficient anticancer effect with ~62% tumor inhibition, which could be attributed to tumor-specific photodynamic therapy. Thus, MPEG-SS-PMLA@Ru micelles could effectively accumulate at the tumor site due to prolonged blood circulation and enhanced permeability and retention (EPR) effect of polymer micelles, releasing Ru complexes under reductive tumor microenvironment and subsequently generating $^1O_2$ to inhibit tumor growth under light.

In the present work, we present an efficient approach for the preparation of PLA-based redox-responsive block copolymers *via* anionic ring-opening polymerization. These block copolymers were capable of self-assembly into micelles in water and used for the incorporation and delivery of Ru complexes. These polymers are composed of amphiphilic polyethylene glycol and phenyl-functionalized polylactide two blocks linked *via* disulfide bond. The hydrophobic block was precisely built by polymerizing lactide (LA) and phenyl-functionalized cyclic lactide (MLA) monomer in order to increase π-π stacking interaction with the Ru complex, which improved the Ru complex loading efficiency (84.3%) and stability of the micelles. The Ru-loaded MPEG-SS-PMLA micelles showed GSH-enhanced *in vitro* release behavior. Compared to the unentrapped Ru complex, the MPEG-SS-PMLA@Ru micelles exhibited efficient cell internalization and intracellular drug release, which eventually led to good PDT effect *in vitro* and *in vivo*. These results suggested that the reasonable design of PLA-based micelles could realize tumor-targeted photosensitizer delivery for cancer phototherapy. We believe that the polymer design provides a new approach to fabricate delivery nanoplatforms with good biosafety and excellent antitumor efficacy.

Declaration of competing interest

The authors declare no conflict of interest.

Acknowledgments

This work was financially supported by the National Science Foundation of China (Nos. 22022803, 22078046, 21808028), Science and Technology Foundation of Liaoning Province (Nos. 2019-BS-047, 2021-YGJC-17), and Fundamental Research Funds for the Central Universities (No. DUT20YG131).

Supplementary materials

Supplementary material associated with this article can be found, in the online version, at doi:10.1016/j.cclet.2022.05.088.

References

[1] S. Zhou, X. Hu, R. Xia, et al., Angew. Chem. Int. Ed. 59 (2020) 23198–23205.
[2] T.C. Pham, V.N. Nguyen, Y. Choi, S. Lee, J. Yoon, Chem. Rev. 121 (2021) 13454–13619.
[3] J. Tian, B. Huang, M.H. Nawaz, W. Zhang, Coord. Chem. Rev. 420 (2020) 213410.
[4] R. Cao, W. Sun, Z. Zhang, et al., Chin. Chem. Lett. 31 (2020) 3127–3130.
[5] F. Heinemann, J. Karges, G. Gasser, et al., Acc. Chem. Res. 50 (2017) 2727–2736.
[6] A. Raza, S.A. Archer, S.D. Fairbanks, et al., J. Am. Chem. Soc. 142 (2020) 4639–4647.
[7] Z. Lv, H. Wei, Q. Li, et al., Chem. Sci. 9 (2018) 502–512.
[8] N. Soliman, L.K. McKenzie, J. Karges, E. Bertrand, et al., Chem. Sci. 11 (2020) 2657–2663.
[9] N. Soliman, G. Gasser, C.M. Thomas, Adv. Mater. 32 (2020) 2003294.
[10] E. Villemin, Y.C. Ong, C.M. Thomas, et al., Nat. Rev. Chem. 3 (2019) 261–282.
[11] K. Ariga, Small Sci. 1 (2020) 2000032.
[12] J. Shen, H.C. Kim, J. Wolfram, et al., Nano Lett. 17 (2017) 2913–2920.
[13] X. Li, Y. Zhang, H. Chen, J. Sun, F. Feng, ACS Appl. Mater. Interfaces 8 (2016) 22756–22761.
[14] M. Appold, C. Mari, C. Lederle, et al., Polym. Chem. 8 (2017) 890–900.
[15] M. He, F. Chen, D. Shao, et al., Biomaterials 275 (2021) 120915.
[16] M. He, G. He, P. Wang, et al., Adv. Sci. 8 (2021) 2103334.
[17] X. Zeng, Y. Wang, J. Han, et al., Adv. Mater. 32 (2020) 2004766.
[18] T.A. Bauer, J. Eckrich, N. Wiesmann, et al., J. Mater. Chem. B 9 (2021) 8211–8223.
[19] G. Boeuf, G.V. Roullin, J. Moreau, et al., ChemPlusChem 79 (2014) 171–180.
[20] W. Sun, S. Li, B. Haupler, et al., Adv. Mater. 29 (2017) 1603702.
[21] N. Kamaly, B. Yameen, J. Wu, et al., Chem. Rev. 116 (2016) 2602–2663.
[22] C. Sun, Y. Liu, J. Du, et al., Angew. Chem. Int. Ed. 55 (2016) 1010–1014.
[23] T. Sim, J.E. Kim, N.H. Hoang, et al., Drug Deliv. 25 (2018) 1362–1371.
[24] X. Guo, X. Wei, Y. Jing, et al., Adv. Mater. 27 (2015) 6450–6456.
[25] S. Aryal, C.M. Hu, L. Zhang, ACS Nano 4 (2010) 251–258.
[26] J. Wang, S. Li, Y. Han, et al., Front. Pharmacol. 9 (2018) 202.
[27] Q. Jin, Y. Deng, X. Chen, J. Ji, ACS Nano 13 (2019) 954–977.
[28] Y. Wang, N. Gong, C. Ma, et al., Nat. Commun. 12 (2021) 1–16.
[29] Z. Liu, T. Cao, Y. Xue, et al., Angew. Chem. Int. Ed. 59 (2020) 3711–3717.
[30] X. Wei, Y. Wang, X. Xiong, et al., Adv. Funct. Mater. 26 (2016) 8266–8280.
[31] H. Qi, Y. Xu, Hu P, et al., Chin. Chem. Lett. 33 (2022) 1131–1140.
[32] X. Gu, Y. Wei, Q. Fan, et al., J. Control. Release 301 (2019) 110–118.
[33] K. Liang, J.E. Chung, S.J. Gao, et al., Adv. Mater. 30 (2018) 1706963.
[34] Y. Liang, X. Deng, L. Zhang, et al., Biomaterials 71 (2015) 1–10.
[35] D. Xi, N. Xu, X. Xia, et al., Adv. Mater. 34 (2021) 2106797.
[36] X. You, L. Wang, L. Wang, J. Wu, Adv. Funct. Mater. 31 (2021) 2100805.
[37] K. Ou, X. Xu, X. Guan, et al., Adv. Funct. Mater. 30 (2020) 1907857.
[38] R. Zhang, R. Nie, T. Fang, et al., Biomacromolecules 23 (2021) 1–19.
[39] D. Li, R. Zhang, G. Liu, Y. Kang, J. Wu, Adv. Healthc. Mater. 20 (2020) 2000605.
[40] L. Tu, Z. Liao, Z. Luo, et al., Exploration 1 (2021) 20210023.
[41] Q. Zhao, C. Huang, F. Li, Chem. Soc. Rev. 40 (2011) 2508–2524.
[42] X. Zhou, M. Xiao, V. Ramu, et al., J. Am. Chem. Soc. 142 (2020) 10383–10399.